Advanced Powder Technology xxx (2014) xxx–xxx

Contents lists available at ScienceDirect

Advanced Powder Technology

journal homepage: www.elsevier.com/locate/apt

Original Research Paper

3D CFD-PBM modeling of the gas–solid flow field in a polydisperse polymerization FBR: The effect of drag model

Ya Yao [a], Yi-Jun He [a], Zheng-Hong Luo [a,*], Lan Shi [b]

[a] Department of Chemical Engineering, School of Chemistry and Chemical Engineering, Shanghai Jiao Tong University, Shanghai 200240, PR China
[b] Research Institute of Petroleum and Chemical Industry, China National Petroleum Corporation (CNPC), Beijing 100195, PR China

ARTICLE INFO

Article history:
Received 9 December 2013
Received in revised form 10 March 2014
Accepted 3 April 2014
Available online xxxx

Keywords:
Polydisperse polymerization FBRs
3-D CFD-PBM model
Drag model
Hydrodynamics

ABSTRACT

This work investigated a coupled computational fluid dynamics and population balance modeling (CFD-PBM) approach to predict the hydrodynamic behavior of the complex gas–solid two-phase flow in a three-dimensional (3-D) polydisperse propylene polymerization fluidized bed reactors (FBRs). Four different drag models, namely Syamlal–O'Brien, Gidaspow, McKeen and EMMS, were incorporated into the CFD-PBM model for evaluating the different effect of drag force between the gas and solid phases. Simulation results revealed a significant effect of the drag model on gas–solid flow in polydisperse polymerization FBRs. It was found that (1) compared to Syamlal–O'Brien and Gidaspow drag models, McKeen and EMMS drag models could predict a lower bed height, a higher temperature and an obvious core-annulus structure in polymerization FBRs; (2) EMMS drag model outperforms the other three drag models with respect to pressure drop prediction; and (3) the drag coefficient had little influence on the evolution of Sauter number and particle-size distribution.

1. Introduction

FBR is one of the most widespread commercial reactors to produce polyolefin due to its simple construction and excellent transfer capabilities [1]. In polyolefin FBRs, continuous-feed small catalyst particles react with the incoming gaseous monomer to produce polydisperse polyolefin particles. It has been recognized that polymerization kinetics, particle growth, aggregation and breakage dynamics could enlarge the polydispersity of particles, which requires the population balance method (PBM) to describe these evolutionary processes for particle size distribution (PSD) modeling [2,3]. Recently, a coupled CFD-PBM model has been developed to simultaneously predict the particle kinetics and the gas–solid flow hydrodynamics in the polyolefin FBRs [4,5].

In the pioneering paper of Fan et al. [6], a two-dimensional (2-D) coupled CFD-PBM approach was developed to model a cold polydisperse polyolefin FBR. Fan et al. [7] also incorporated the chemical reaction engineering (CRE) model into the 2-D CFD-PBM model to investigate roles of intrinsic kinetics and catalyst PSD in the gas–solid polyolefin FBR. Recently, based on Fan et al.'s works [6,7], Luo's group at Xiamen University and Shanghai Jiao Tong University developed a 3-D CFD-PBM model to describe the gas–solid flow in a polypropylene FBR [4]. More recently, this group further incorporated a single particle model into the CFD-PBM model for investigating the effect of intraparticle transfer limitation on the gas–solid flow behavior in the polypropylene FBR [5]. The previous works proved that the CFD-PBM approach is effective for describing the gas–solid flow behavior in polydisperse polyolefin FBRs. Note that these previous developed CFD-PBM models are based on the Euler-Euler approach [4–7].

In the Euler–Euler approach, both the gas and the solid phases are treated mathematically as interpenetrating continua, and mass and momentum conservation equations for each phase are derived [8]. Coupling is achieved via the inter-phase forces including drag force, lift force and virtual mass force. In FBRs, the drag model plays an important role in gas–solid two-phase flow modeling [9,10]. The available drag models can be broadly classified into two categories: (i) the conventional drag models [11–13] and (ii) the structure-based drag models [14–20]. The conventional drag models are derived using the terminal velocity data for a single particle and pressure drop data from a dense packed bed [9]. Since the gas–solid flows in FBRs are inherently unstable and manifest fluctuations, which results from gas–solid interactions, some structure-based drag models linking to the fluctuations were suggested, such as McKeen drag model [14] and EMMS drag model [15–20]. To date, there are many published papers relating to the applications of these drag models [9,10,14–16,21–23]. Comparative

* Corresponding author. Tel./fax: +86 21 54745602.
E-mail address: Luozh@sjtu.edu.cn (Z.-H. Luo).

http://dx.doi.org/10.1016/j.apt.2014.04.001
0921-8831/

Nomenclature

C	drag equation scale factor in McKeen drag model
C_D	drag coefficient
$C_{p,g}$	heat capacity coefficient of gas phase (kJ kg^{-1} K^{-1})
$C_{p,s}$	heat capacity coefficient of solid phase (kJ kg^{-1} K^{-1})
$[C^*]$	active catalyst site concentration (kmol kg$_{cat}^{-1}$)
d_s	particle diameter (m)
g	gravitational acceleration (m s^{-2})
H	bed height (m)
h_i	specific enthalpy of the ith phase (kJ kg^{-1} K^{-1})
$\bar{\bar{I}}$	identity matrix
kk	specified number of moments
KK	an aggregation rate constant (m^{-6} s^{-1})
L_i, L_j	particle diameter (m)
$[M]$	monomer concentration (mol m^{-3})
$\dot{m}_{sp}$	mass transfer between the gas and solid phase
Nu_s	Nusselt number of solid phase, dimensionless
N	the number of quadrature nodes
ΔP_s	pressure drop described by the buoyant weight of the suspension (K Pa)
ΔP_g	the effect of gas phase weight on the pressure weight (K Pa)
Pr	Prandtl number of liquid phase
Q_{gs}	intensity of heat exchange between gas and solid phases (W s^{-1} m^{-3})
q_i	the heat flux (W m^{-2})
Re_s	Reynolds number
T	time (s)
T_s	solid temperature (K)
T_{sf}	the average polymer melting temperature (K)
T	solid temperature (°C)
$\vec{v}_g$	gas velocity (m/s)
$\vec{v}_s$	particle velocity (m/s)
$\vec{v}_p$	velocity of phase p (m/s)
x	spatial coordinate (m)

Greek symbols

α_g	volume fraction of gas phase
α_s	volume fraction of solid phase
α_q	volume fraction of phase q
$a(L_i, L_j)$	aggregation kernel
β	inter-phase momentum transfer coefficient (kg/(m^3 s))
μ_g	viscosity of gas phase (Pa s)
μ_s	solid shear viscosity (Pa s)
ρ_g	density of gas mixture (kg/m^3)
ρ_s	density of solid (kg/m^3)
ρ_q	density of phase q (kg/m^3)
$\bar{\bar{\tau}}_g$	shear stress for gas phase (N/m^2)
$\bar{\bar{\tau}}_s$	shear stress for solid phase (N/m^2)
λ_s	solid bulk viscosity (Pa s)
ϕ	medium porosity
κ_i	thermal conductivity for phase i (W m^{-1} K^{-1})
ω	the correction factor in EMMS drag model
$\Delta Q_{rs\alpha}$	heat produced from polymerization reaction (kJ kmol^{-1})

Subscripts

g	gas phase
s	solid phase

analysis of drag models for FBRs has also been reported [9,10]. For instance, Li et al. [9] examined the suitability of four drag models, namely Syamlal–O'Brien, Gidaspow, modified Syamlal–O'Brien and McKeen for predicting the hydrodynamics of the turbulent fluidization of FCC particles. Loha et al. [10] assessed four drag force models, namely Syamlal–O'Brien, Gidaspow, EMMS, and McKeen in simulating bubbling fluidized bed hydrodynamics. However, in these works [9,10], the polydispersity of the solid phase was ignored and the examination was performed in a CFD model instead of a CFD-PBM model. In addition, although Fan et al. [6,7] and Luo's group [4,5,24] simulated polydisperse polyolefin FBR hydronamics using the CFD-PBM models, only the conventional Gidaspow drag model was applied. The effect of different drag models was not investigated numerically in their works [4,5,24]. To the best of our knowledge, there is so far no open literature on assessment of different drag models in simulating the hydrodynamics of the gas–solid flow in a polydisperse polymerization fluidized bed.

In this study, a 3-D CFD-PBM modeling approach has been proposed to investigate the gas–solid hydrodynamics in a polydisperse propylene polymerization FBR. The coupled model is based on the Eulerian–Eulerian two-fluid model and involves the kinetic theory of granular flow, the population balance and the heat exchange equations. Four representative drag models (i.e., Syamlal–O'Brien, Gidaspow, EMMS and McKeen) are incorporated in the coupled model to compare their different effects on the bed hydrodynamics. Some of the results are also validated with classical calculation.

2. Mathematical model and numerical simulations

2.1. Simulated reactor

To obtain the effect of the drag force model on the gas–solid polydisperse polymerization fluidized bed hydrodynamics, an experiment-scale FBR was studied as in our previous works (see Fig. 1) [4,5,24,25].

2.2. Material and simulation methods

2.2.1. The CFD-PBM model and the drag force models

The 3-D CFD-PBM model is analogous to that reported in our previous work [4] with minor difference. The difference is the drag force model used in the CFD-PBM model. Besides the conventional Gidaspow drag model [4], Syamlal–O'Brien, EMMS and McKeen drag models are applied herein. For the detailed description of

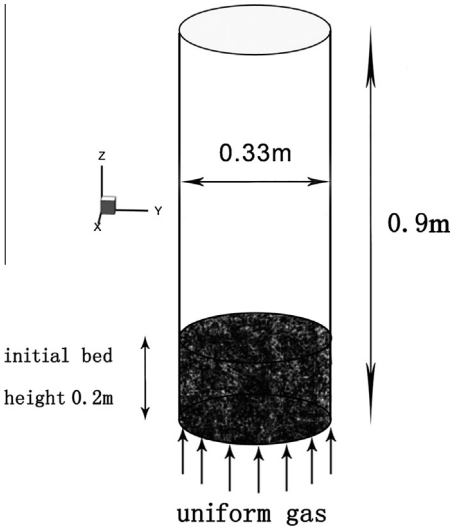

Fig. 1. Geometrical features of the simulated FBR.

the 3-D CFD-PBM model, the readers are encouraged to refer to Chen et al.'s work [4]. For the convenience, several major equations are still listed as follows.

2.2.1.1. Eulerian–Eulerian two-fluid equation. The continuity equation for phase q ($q = g$ for gas, s for solid phase) is:

$$\frac{\partial}{\partial t}(\alpha_q \rho_q) + \nabla \cdot (\alpha_q \rho_q \vec{v}_q) = \dot{m}_{sp} \tag{1}$$

The momentum conservation equations for gas and solid phases can be written as:

$$\frac{\partial}{\partial t}(a_g \rho_g \vec{v}_g) + \nabla \cdot (a_g \rho_g \vec{v}_g \cdot \vec{v}_g) = -a_g \nabla p + \nabla \cdot \bar{\bar{\tau}}_g + \beta(\vec{v}_s - \vec{v}_g) + a_g \rho_g g \tag{2}$$

$$\bar{\bar{\tau}}_g = \alpha_g \mu_g (\nabla \vec{v}_g + \nabla \vec{v}_g^T) \tag{3}$$

$$\frac{\partial}{\partial t}(\alpha_s \rho_s \vec{v}_s) + \nabla \cdot (\alpha_s \rho_s \vec{v}_s \vec{v}_s) = -\alpha_s \nabla p - \nabla p_s + \nabla \cdot \bar{\bar{\tau}}_s + \beta(\vec{v}_g - \vec{v}_s) + \alpha_s \rho_s g \tag{4}$$

$$\bar{\bar{\tau}}_s = \alpha_s \mu_s (\nabla \vec{v}_s + \nabla \vec{v}_s^T) + \alpha_s \left(\lambda_s - \frac{2}{3}\mu_s\right) \nabla \cdot \vec{v}_s \bar{\bar{I}} \tag{5}$$

The energy balance equation for gas and solid phases are expressed as:

$$\frac{\partial}{\partial t}(\alpha_g \rho_g h_g) + \nabla \cdot (\alpha_g \rho_g v_g h_g) = -\alpha_g \frac{\partial p_g}{\partial t} + \bar{\bar{\tau}}_g : \nabla v_g - \nabla \cdot q_g + \sum_{p=1}^{n} (Q_{gs} + \dot{m}_{gs} h_{gs} - \dot{m}_{sg} h_{sg}) \tag{6}$$

$$\frac{\partial}{\partial t}(\alpha_s \rho_s h_s) + \nabla \cdot (\alpha_s \rho_s v_s h_s) = -\alpha_s \frac{\partial p_s}{\partial t} + \bar{\bar{\tau}}_s : \nabla v_s - \nabla \cdot q_s + \sum_{p=1}^{n} (Q_{sg} + \dot{m}_{sg} h_{sg} - \dot{m}_{gs} h_{gs}) + \Delta Q_{rs\alpha} \tag{7}$$

where

$$h_i = \int_{T_{ref}}^{T} c_{p,i} dT \quad i = g \text{ or } s \tag{8}$$

$$q_i = -\alpha_i \kappa_i \nabla T_i, \quad i = g \text{ or } s \tag{9}$$

2.2.1.2. Heat-exchange coefficient. The rate of energy transfer between phases is described as follow:

$$Q_{gs} = \kappa_{gs}(T_s - T_g) \tag{10}$$

$$\kappa_{gs} = \frac{6\kappa_g \alpha_g \alpha_s \mathrm{Nu}_s}{d_s^2} \tag{11}$$

We applied the correlation of Ranz–Marshall [37] to determine the Nusselt number as follow:

$$\mathrm{Nu}_s = 2.0 + 0.6\mathrm{Re}_s^{1/2}\mathrm{Pr}^{1/3} \tag{12}$$

$$\mathrm{Pr} = \frac{c_{p,s}\mu_s}{\kappa_s} \tag{13}$$

2.2.1.3. The Syamlal–O'Brien drag model. According to Eq. (4), $\beta(\rightarrow v_g - \rightarrow v_s)$ is the interaction force between the gas and solid phases, which greatly affects the hydrodynamic behavior in FBRs. Different drage models propose different equations for computing inter-phase momentum transfer coefficient (β).

Syamlal and O'Brien [12] proposed a drag model based on measurements of the terminal velocities of particles in fluidized or settling beds expresses as follow:

$$\beta = \frac{3}{4}\frac{\alpha_s \alpha_g \rho_g}{v_{r,s}^2 d_s} C_D |\vec{v}_s - \vec{v}_g| \tag{14}$$

where $v_{r,s}$ is the terminal velocity correlation for the solid phase. Namely,

$$v_{r,s} = 0.5(A - 0.06\mathrm{Re}_s + \sqrt{(0.06\mathrm{Re}_s)^2 + 0.12\mathrm{Re}_s(2B - A) + A^2}) \tag{15}$$

$$A = \alpha_g^{4.14}, \quad B = \begin{cases} 0.8\alpha_g^{1.28} & \alpha_g \leqslant 0.85 \\ \alpha_g^{2.65} & \alpha_g \leqslant 0.85 \end{cases} \tag{16}$$

2.2.1.4. The Gidaspow drag model. Gidaspow et al. [13] combined the Ergun equation [26] using for dense phase calculation with the Wen–Yu equation [11] using for dilute phase calculation.

$$\beta = 150\frac{\alpha_s^2 \mu_g}{\alpha_g d_s^2} + 1.75\frac{\alpha_s \rho_g |\vec{v}_s - \vec{v}_g|}{d_s} \quad \text{for } \alpha_g < 0.8 \tag{17}$$

$$\beta = \frac{3}{4} C_D \frac{\alpha_s \alpha_g \rho_g |\vec{v}_s - \vec{v}_g|}{d_s} \alpha_g^{-2.65} \quad \text{for } \alpha_g \geqslant 0.8 \tag{18}$$

where

$$C_D = \begin{cases} \frac{24}{\alpha_g \mathrm{Re}_s}[1 + 0.15(\alpha_g \mathrm{Re}_s)^{0.687}] & \mathrm{Re}_s \leqslant 1000 \\ 0.44 & \mathrm{Re}_s > 1000 \end{cases} \tag{19}$$

2.2.1.5. The McKeen drag model. McKeen et al. [14] modified the Gibilaro drag model [27] using a scale factor C as follows:

$$\beta = C\left(\frac{17.3}{\mathrm{Re}_s} + 0.336\right)\frac{\rho_g |\vec{v}_s - \vec{v}_g|}{d_s} a_s a_g^{-1.8} \tag{20}$$

When one considers the effect of interparticle cohesive forces, the drag will decrease. Therefore, the value of C is taken as 0.15 in present work.

2.2.1.6. The EMMS drag model. Yang et al. [15] proposed a new drag model based on energy minimization multi-scale (EMMS). To describe the reduction of drag coefficient caused by the particle aggregation, a correction factor (ω) was introduced. The EMMS model has been widely used in CFD simulations and was verified by many cases. For instance, Du et al. [28] thought that the EMMS drag model could be capable of reflecting the real mechanisms of gas–solid interactions. The main equations are listed as follows:

$$\beta = \frac{3}{4}\frac{\alpha_s \alpha_g \rho_g |\vec{v}_s - \vec{v}_g|}{d_s} C_D \omega \quad \text{for } \alpha_g \geqslant 0.74 \tag{21}$$

$$\beta = 150\frac{\alpha_s^2 \mu_g}{\alpha_g d_s^2} + 1.75\frac{\alpha_s \rho_g |\vec{v}_s - \vec{v}_g|}{d_s} \quad \text{for } \alpha_g < 0.74 \tag{22}$$

The correction factor ω is expressed as

$$\omega(a_g) = \begin{cases} -0.5760 + \frac{0.0214}{4(a_g - 0.7463)^2 + 0.0044} & (0.74 \leqslant a_g \leqslant 0.82) \\ -0.0101 + \frac{0.0038}{4(a_g - 0.7789)^2 + 0.0040} & (0.82 < a_g \leqslant 0.97) \\ -31.8295 + 32.8295 a_g & (a_g > 0.97) \end{cases} \tag{23}$$

Please cite this article in press as: Y. Yao et al., 3D CFD-PBM modeling of the gas–solid flow field in a polydisperse polymerization FBR: The effect of drag model, Advanced Powder Technology (2014), http://dx.doi.org/10.1016/j.apt.2014.04.001

2.2.1.7. The population balance method. The general form of the PBE is:

$$\frac{\partial n(L;x,t)}{\partial t}+\nabla\cdot[\vec{u}(L;x,t)]=-\frac{\partial}{\partial L}[G(L)n(L;x,t)]+B_{ag}(L;x,t)-D_{ag}(L;x,t)+B_{br}(L;x,t)-D_{br}(L;x,t) \quad (24)$$

where $n(L;x,t)$, $B_{ag}(L;x,t)$, $D_{ag}(L;x,t)$, $B_{br}(L;x,t)$, $D_{br}(L;x,t)$ are the number density function of particles, the birth and death rate of particles due to aggregation, the birth and death rate of particles due to breakage, respectively.

The moments of the PSD are defined as:

$$m_{kk}(x,t)=\int_0^\infty n(L;x,t)L^{kk}dL \quad kk=0,1,\ldots,N-1 \quad (25)$$

Incorporating Eq. (25) into Eq. (24) results in:

$$\frac{\partial}{\partial t}(m_{kk})+\nabla\cdot(\vec{u}m_{kk})=-\int_0^\infty kkL^{kk-1}G(L)n(L;x,t)dL+B_{ag,kk}(L;x,t)-D_{ag,kk}(L;x,t)+B_{br,kk}(L;x,t)-D_{br,kk}(L;x,t) \quad (26)$$

The quadrature method of moments (QMOM) which uses a quadrature approximation as follow is used to solve the PBE in this study:

$$m_{kk}\approx\sum_{i=1}^{N}w_iL_i^{kk} \quad (27)$$

By introducing the quadrature approximation, Eq. (25) can be written as:

$$\frac{\partial}{\partial t}(m_{kk})+\nabla\cdot(\vec{u}m_{kk})=kk\sum_{i=1}^{N}L^{kk-1}G(L_i)w_i+\frac{1}{2}\sum_{i=1}^{N}\sum_{j=1}^{N}w_iw_j(L_i^3+L_j^3)^{kk/3}\beta_{ij}-\sum_{i=1}^{N}\sum_{j=1}^{N}w_iw_jL_i^{kk}\beta_{ij}+\sum_{i=1}^{N}w_ia_i^*\bar{b}_i^{(kk)}-\sum_{i=1}^{N}w_iL_i^{kk}a_i^* \quad (28)$$

The growth rate $G(L_i)$ is related to the polymerization reaction rate, and is expressed as:

$$G(L_i)=\frac{R_pL_0^3}{3\rho_sL_i^2} \quad (29)$$

where R_p is the polymerization reaction rate defined based on Zacca et al.'s equation [38]. R_p is shown as

$$R_p=k_{p0}\exp\left(-\frac{E}{R(273.15+t)}\right)[M][C^*] \quad (30)$$

2.3. Simulation conditions and modeling method

The simulated results are dependent on the range of parameter values presented in the CFD-PBM model. Most of the parameters linked to the properties of the gas and solid phases in the reactor were reported in our previous works [4,5,25]. The previous parameter values are still used herein [4,5,25]. The parameters used for the simulations are shown in Tables 1 and 2. The initial PSD with mean particle size of 0.0002 m is shown in Fig. 2.

The 3-D simulations based on the CFD-PBM model were performed with the commercial CFD package FLUENT 6.3.26 (Ansys Inc., US) in double precision mode. A commercial grid-generation tool, GAMBIT 2.3.16 (Ansys Inc., US) was used to generate the 3-D geometries and the grids. Grid sensitivity was carried out previously, where indicated that a total amount of 89,010 cells was adequate to conserve the mass of solid phase in the dynamics model [4,5,25]. The phase coupled SIMPLE algorithm [29] was used to couple pressure and velocity. Equations and source terms of the reaction kinetics and PBM were defined via external user-defined scalars (UDS) and functions (UDF). A two-stage calculation was implemented [4,25]. The time-averaging has been done between 1.5 s and 3 s to obtain the time-averaged value. Furthermore, the simulations were performed in a platform of 4× Intel Xeon E7 Series with 64 GB of RAM.

3. Results and discussion

The effects of different drag models on flow characteristics under cold-flow condition are first investigated. Then, the polymerization reaction is added, and the temperature distributions and the evolutions of the PSD are comapred using four drag models.

3.1. The time to reach stable fluidization stage

Fig. 3 shows the fluidization process from 0.1 s to 2.0 s using Gidaspow drag model. It clearly reveals that the whole bed can be considered steady-state after 1.5 s. Therefore, it is reasonable to assume that the related variables basically keep constant after 1.5 s. Similarly, the time-averaged values used in the following sections are collected from 1.5 to 3.0 s.

3.2. The fluidization process

First, we simulated the fluidization process using four drag models, respectively. Since it is observed that the predicted flow structures before 0.3 s are basically the same for all four drag models, Fig. 4 only shows the flow structures starting from 0.3 s.

It can be seen from Fig. 4 that both Syamlal–O'Brien and Gidaspow drag models show a similar fluidization phenomenon in the whole fluidization period (0–1.5 s). Fig. 4(a) and (b) show that (1) the whole bed moves up in the initial period (0–0.6 s); (2) the bubbles form at 0.6 s and move along the gas flow direction, which will result in a uniformly mixing of the particles; and (3) the bed achieves a complete fluidization at 1.5 s, which is the same as McKeen and EMMS drag models. In addition, a similar behavior of the bubbles is also observed using EMMS drag model, while using McKeen drag model, the predicted gas goes upward in the way of emulsion rather than bubble since 0.6 s. Fig. 4(d) shows that EMMS drag model exists the most obvious bubble interface and bed upper surface. It is also observed that the predicted bed heights using both McKeen and EMMS drag models are lower than that of using Syamlal–O'Brien and Gidaspow drag models. In practice, the first two models consider the meso-scale structure existing in the form of particle clusters or strands in the system, which leads to a relative stable fluidization process. Indeed, the clustering nature of the FBR system has been widely corroborated in other literatures [14,15]. Note that the drag coefficient for a control volume strongly depends on this heterogeneous structure [15].

Fig. 4 implies that the predicted hydrodynamics by EMMS drag model is approximate in agreement with the reality. Fig. 4 also reveals that the fluidization is much asymmetric compared to the simulated results using only CFD model [25], which implies that the coupled CFD-PBM approach could be more suitable for simulating more complicated and ruleless polydispersed flow.

3.3. The pressure drop under cold-flow condition

The pressure drop is one of the most important parameter in the successful scale up of FBRs, which is always described by the buoyant weight of the suspension calculated as [31–33]:

$$\Delta P_s=(\rho_s-\rho_g)(1-\phi)gH \quad (31)$$

Please cite this article in press as: Y. Yao et al., 3D CFD-PBM modeling of the gas–solid flow field in a polydisperse polymerization FBR: The effect of drag model, Advanced Powder Technology (2014), http://dx.doi.org/10.1016/j.apt.2014.04.001

Table 1
Physical property of gas and solid phases and operation conditions.

d_s (m)	ρ_s (kg m^{-3})	ρ_g (kg m^{-3})	μ_g (Pa s)	$C_{p,g}$ (J kg^{-1} K^{-1})	$C_{p,s}$ (J kg^{-1} K^{-1})	Composition (V/V)
Sauter	910.0	21.56	1.081×10^{-5}	1817	2104	C_3H_6:Air = 6:1

Table 2
Main model parameters.

Descriptions	Values
Turbulence model	k–ε (RNG, dispersed)
Granular viscosity	Gidaspow et al. [13]
Granular bulk viscosity	Lun et al. [30]
Frictional viscosity	Schaeffer
Angle of internal friction	30°
Granular temperature	Algebraic
Inlet boundary condition	Velocity inlet
Outlet boundary condition	Pressure outlet
Wall boundary condition	No slip for air, free slip for solid phase, the adiabatic heat-transfer equation
Initial bed height	0.2 m
Initial volume fraction of solid phase	0.63
Operating pressure	1.40×10^6 Pa
Inlet gas velocity	0.3 m s^{-1}
Inlet gas temperature	313 K
Restitution coefficient	0.9
Turbulent kinetic energy	0.00036 m^2/s^2
Turbulent dissipation rate	8.2×10^{-5} m^2/s^3
Maximum iterations	50
Convergence criteria	1×10^{-4}
Time step	1×10^{-3} s

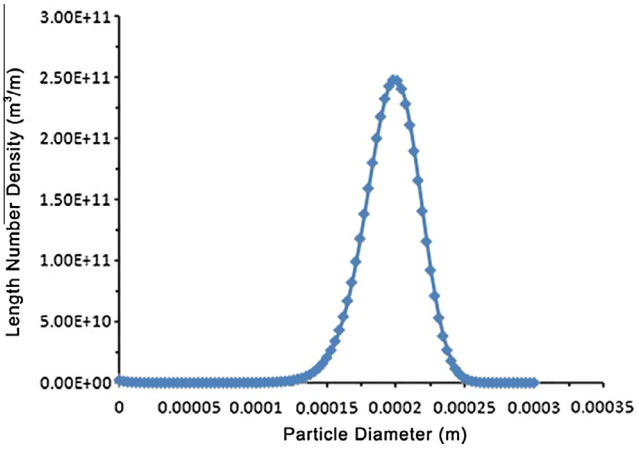

Fig. 2. The initial PSD profile.

As the gas phase density is up to 21.56 kg m^{-3} in this study. It is necessary to consider the effect of gas phase weight on the pressure drop:

$$\Delta P_g = \phi \rho_g g H \tag{32}$$

Fig. 5 shows the values of pressure drop obtained by both theoretical equation and numerical simulation. The calculated value by classical Eqs. (31) and (32) is 1246 Pa, which is approximately in agreement with that obtained by simulation results. However, the pressure drop exist fluctuations caused by the violent motions of particles in the actual bed.

According to Fig. 5, the fluctuation around a mean value using the EMMS drag model can fit the calculated data best. The time-averaged pressure drop between 1.5 s and 3 s using Syamlal–O'Brien, Gidaspow, McKeen and EMMS models are 1254, 1260, 1250 and 1245 Pa, respectively. Obviously, the mean value obtained under EMMS model is the closest to the calculated value. It means that using the EMMS drag model, the predicted pressure drop is the most accurately.

3.4. The time-averaged solid volume fraction distribution

In order to perform a complete comparison, we chose five typical bed heights evenly across the whole FBR, i.e., H = 0.05, 0.15, 0.25, 0.35 and 0.45 m. Fig. 6 illustrates the comparison of the simulated time-averaged solid volume fraction coutour for four drag models. Both the solid volume fraction distributions predicted using Syamlal–O'Brien and Gidaspow drag models are very homogeneous. It is obvious that this phenomenon is not in agreement with the actual results in FBRs [34]. However, the obvious existence of core-annular structure of the flow in the FBR is predicted using McKeen and EMMS drag models, which is in qualitative agreement with the simulated results obtained by other researchers [10,14,15]. Indeed, in actual fluidization, the particles have a tendency to attach to the wall, which leads to a core-annular structure of the flow in the FBR. Because of the consideration of the meso-scale structure, McKeen and EMMS drag models can reflect this fluidization structure well.

3.5. The time-averaged vertical solid velocity distribution

Fig. 7 shows the comparison of the simulated time-averaged vertical solid velocity distributions in five typical bed height using different drag models. In general, due to the existence of the core-annular structure in FBRs, the particles move up in the central region and fall down along the wall in the annular region. It leads to backmixing in FBRs [35]. The backmixing phenomenon can't be predicted well by McKeen drag model. When using Syamlal–O'Brien and Gidaspow drag models, the solid velocity upward is large at the height of 0.45 m. However, using the EMMS drag model, a less value of vertical solid velocity can be obtained at the same bed height. The above results obtained from Fig. 7 also match the phenomenon observed from Fig. 4. As described earlier, using Gidaspow and Syamlal–O'Brien drag models, the simulated particle flow is more violent than that obtained using the EMMS drag model. In conclusion, the solid velocity distribution predicted by Syamlal–O'Brien, Gidaspow and EMMS drag models are all rational, and only the McKeen model deviates from the actual situation.

3.6. The sold phase temperature distribution

Due to the addition of the highly exothermic polymerization in FBRs, the temperature distribution should be recorded. Herein, the predicted solid phase temperature distributions using the four drag models are shown in Fig. 8. It is seen from Fig. 8 that the total temperature data for McKeen and EMMS drag models are higher than those for the other two models. This is due to the fact that the fluidization is more violent by using Syamlal–O'Brien and Gidaspow drag models, which would cause a higher bed height. Accordingly, it would lead to a larger porosity and less local released heat.

Furthermore, Fig. 8 shows that the rise in temperature with the bed height predicted by Syamlal–O'Brien and Gidaspow drag models are comparative smaller. This is due to the fact that larger porosity would lead to faster heat transfer. In the actual polymerization process, the particle temperature in the bottom of FBRs is lower caused by the feeding of the cold fresh gaseous monomers

Please cite this article in press as: Y. Yao et al., 3D CFD-PBM modeling of the gas–solid flow field in a polydisperse polymerization FBR: The effect of drag model, Advanced Powder Technology (2014), http://dx.doi.org/10.1016/j.apt.2014.04.001

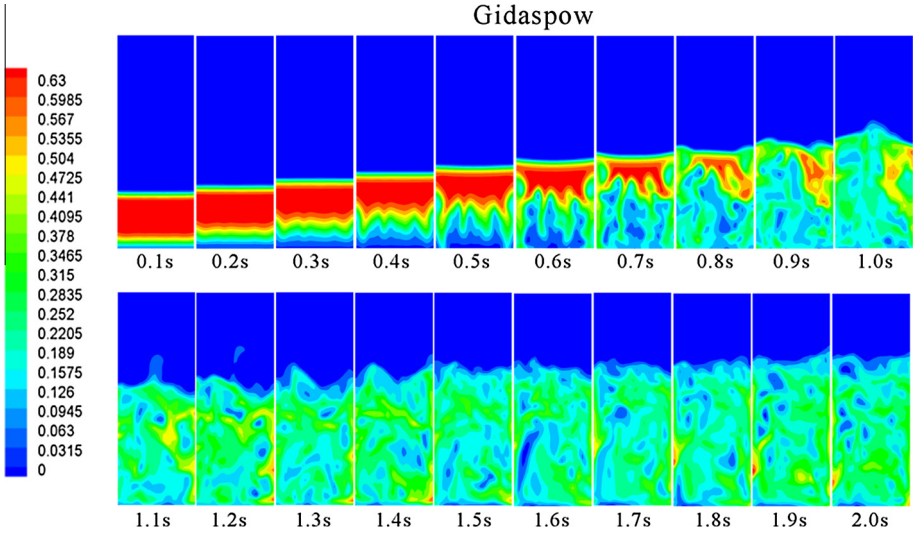

Fig. 3. The fluidization process using Gidaspow model.

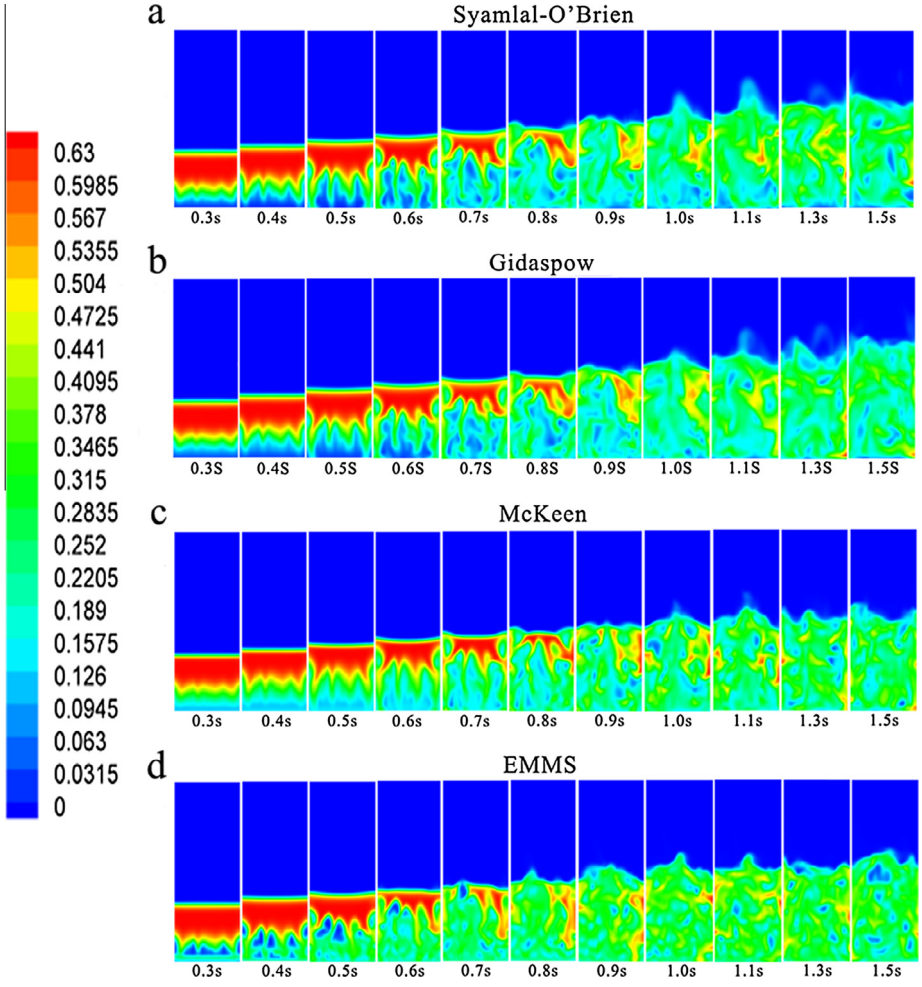

Fig. 4. The fluidization process in the FBR.

(313.15 K). Since the olefin polymerization is a highly exothermic reaction, the temperature will increase along the axial direction from the bottom to the top in the FBRs. Note that the excellent heat transfer capability of the FBRs would avoid hot spot in the bed. However, an uneven temperature distribution is still observed due to the presence of PSD and polymerization kinetics. Moreover, the particles are easy to aggregate near the wall, which consequently leads to the highest temperature near the wall in FBRs.

Please cite this article in press as: Y. Yao et al., 3D CFD-PBM modeling of the gas–solid flow field in a polydisperse polymerization FBR: The effect of drag model, Advanced Powder Technology (2014), http://dx.doi.org/10.1016/j.apt.2014.04.001

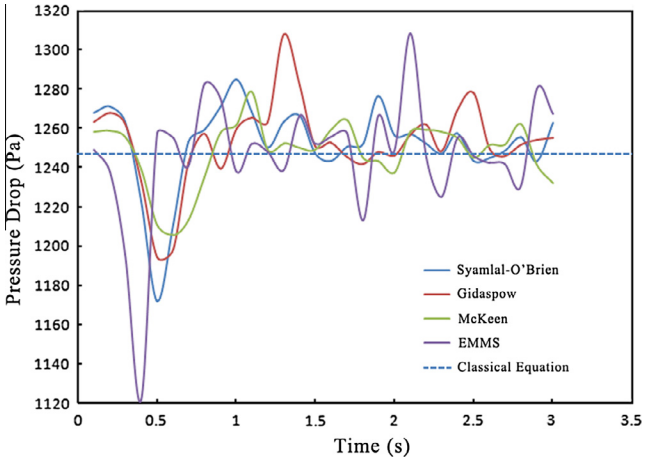

Fig. 5. The pressure drop with the fluidization proceeding in the FBR.

Unfortunately, the experimental data of FBRs with polymerization is difficult to obtain. So we have to use this section just as an assistant analysis.

3.7. The PSD distribution

Since the PBM is coupled with the CFD model, the drag model will influence the PSD in FBRs [4]. Herein, the effect of the drag model on the PSD is also predicted. Since our simulation results illustrated that the effects of the drag model on the PSD at different fluidization time points (>1.5 s) are basically the same, only one fluidization time (i.e., t = 14.0 s) is selected for PSD prediction.

Fig. 9(a) shows the effects of the four drag models on the PSD prediction. It is observed that four PSD curves are almost the same, which means that the drag model has little influence on the PSD in this simulation. This is due to the fact that the effect of particle size on the aggregation rate is not included in our current work. Compared to Luo et al.'s model, the model developed by Hatzantonis

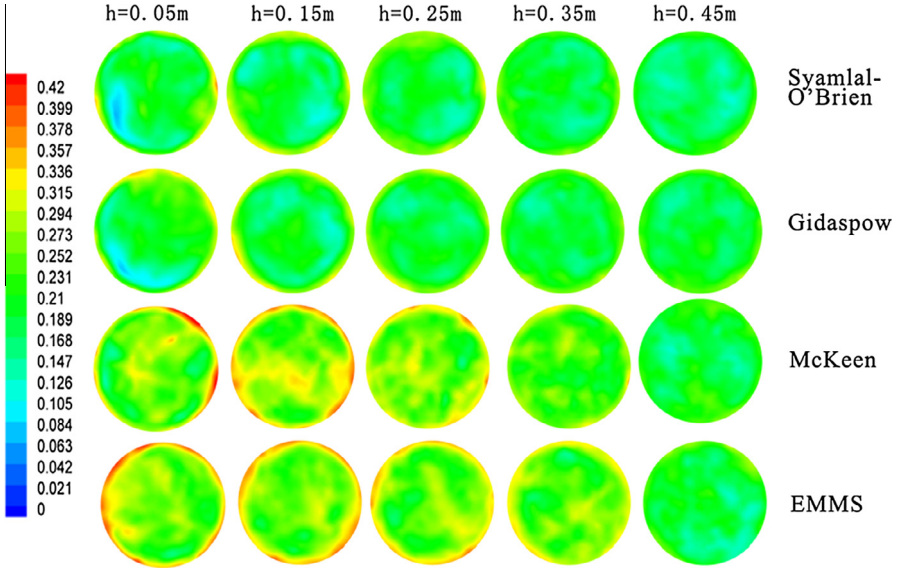

Fig. 6. The time-averaged solid volume fraction distributions in the FBR.

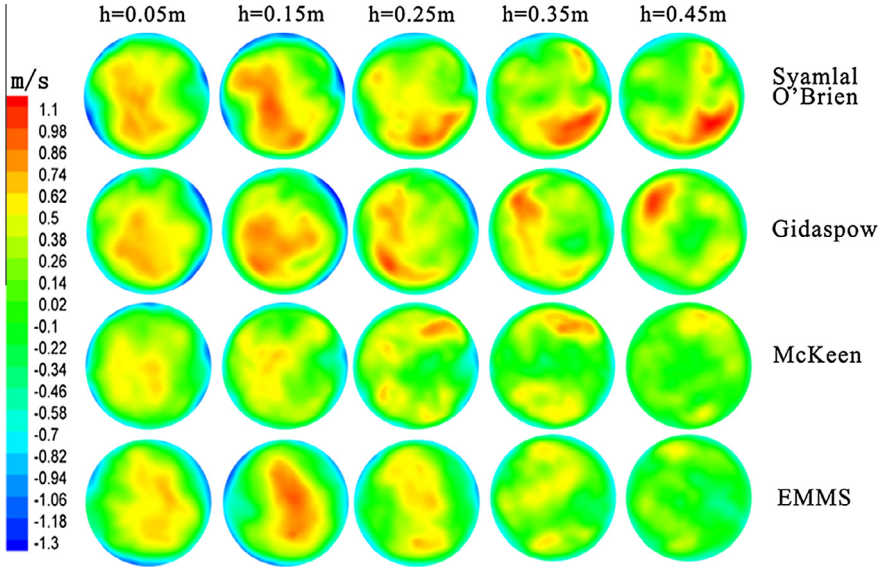

Fig. 7. The time-averaged vertical solid velocity distributions in the FBR.

Please cite this article in press as: Y. Yao et al., 3D CFD-PBM modeling of the gas–solid flow field in a polydisperse polymerization FBR: The effect of drag model, Advanced Powder Technology (2014), http://dx.doi.org/10.1016/j.apt.2014.04.001

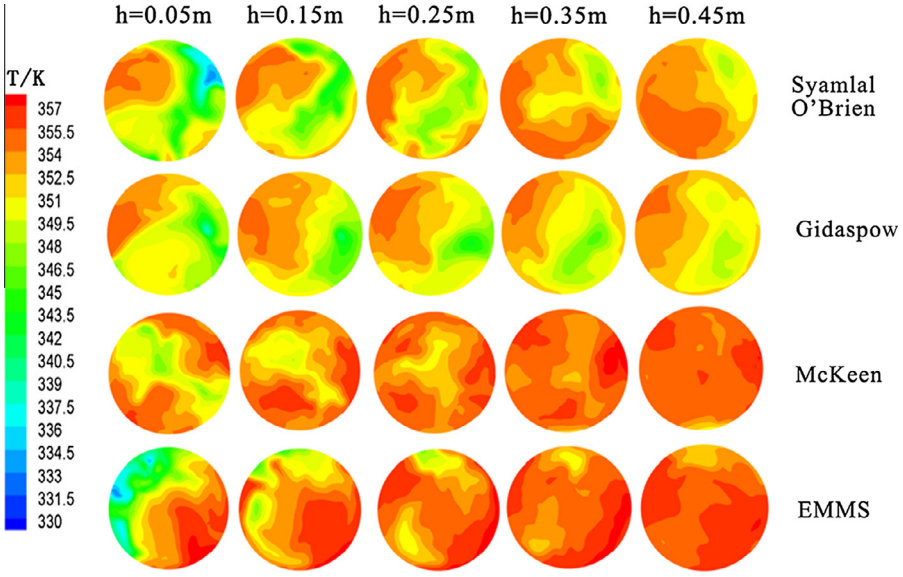

Fig. 8. The solid phase temperature distributions in the FBR.

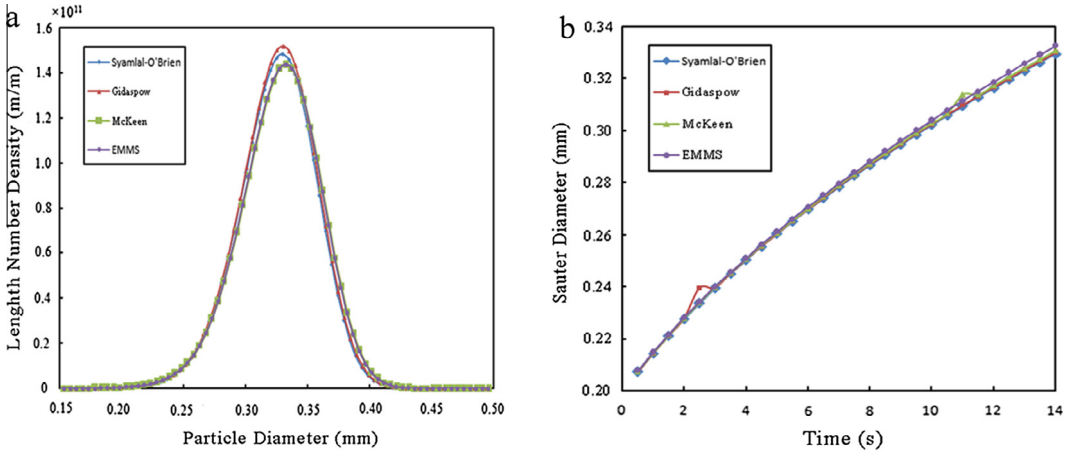

Fig. 9. (a) The PSD (t = 8.5 s), and (b) the evolution of the Sauter diameter with the fluidization proceeding in the FBR.

et al. [36] and Yiannoulakis et al. [2] is much more accurate (the simulated result using Hatzantonis model can be obtained from Fig. 4 in Chen et al.'s work [4]). The model is expressed as

$$a(L_i, L_j) = KK(L_i^2 + L_j^2)\left(\frac{1}{L_i L_j}\right)^4 \tag{33}$$

$$KK = kk_1 \exp(kk_2 T_s / T_{sf}) \tag{34}$$

The above model can exactly reflect the influence of the particle-size on the aggregation rate and the exponentially increasing of the aggregation rate with the particle surface temperature [4,5,24,25]. However, the parameters in Hatzantonis et al.'s model are difficult to determine. Since the value of KK being difficult to determine through the experiment shows a great influence on the aggregation rate, we still choose Luo et al.'s model in this work.

4. Conclusion

In this study, a 3D CFD-PBM coupled model was applied to predict the effect of the drag model on the gas–solid two-phase flow in polydisperse polymerization FBRs. Four representative drag models, i.e., Syamlal–O'Brien, Gidaspow, EMMS, and McKeen, were thoroughly compared.

The results show that the drag model has a significant effect on the hydrodynamic behavoir of gas–solid flow in polydisperse polymerization FBRs. It is found that (1) compared to Syamlal–O'Brien and Gidaspow drag models,McKeen and EMMS drag models show a lower bed height, a higher temperature and an obvious core-annulus structure in polymerization FBRs, while both Syamlal–O'Brien and Gidaspow drag models cannot predict core-annulus structure; (2) the predicted pressure drop using EMMS drag model give the best fit to that calculated by the classical Eq. (3) the back-mixing phenomenon cannot be predicted well by McKeen drag model; (4) Syamlal–O'Brien and Gidaspow drag models show larger upward solid velocity than that by EMMS drag model, and the total temperature for McKeen and EMMS drag models are higher than those for the other two models; and (5) the drag coefficient has little influence on the evolution of Sauter number and PSD.

Based on the above discussion, the more complex hydrodynamics for the EMMS drag model can be obtained, which may be really in reality.

Further studies on the CFD-PBM coupled model for the gas–solid two-phase flow in FBR are in progress in our group.

Please cite this article in press as: Y. Yao et al., 3D CFD-PBM modeling of the gas–solid flow field in a polydisperse polymerization FBR: The effect of drag model, Advanced Powder Technology (2014), http://dx.doi.org/10.1016/j.apt.2014.04.001

Acknowledgments

The authors thank the National Natural Science Foundation of China (No. 201076171), the State-Key Laboratory of Chemical Engineering of Tsinghua University (No. SKL-ChE-13A05), the Key Laboratory of Advanced Control and Optimization for Chemical Processes of the National Ministry of Education of China (No. 2012ACOCP03) and the State Key Laboratory of Coal Conversion of China (No. J13-14-102) for supporting this work.

References

[1] A. Ahmadzadeh, H. Arastoopour, F. Teymour, M. Strumendo, Population balance equations' application in rotating fluidized bed polymerization reactor, Chem. Eng. Res. Des. 86 (2008) 329–343.
[2] H. Yiannoulakis, A. Yiagopoulos, C. Kiparissides, Recent developments in the particle size distribution modeling of fluidized-bed olefin polymerization reactors, Chem. Eng. Sci. 56 (2001) 917–925.
[3] Z.H. Luo, P.L. Su, X.Z. You, D.P. Shi, J.C. Wu, Steady-state particle size distribution modeling of polypropylene produced in tubular loop reactors, Chem. Eng. J. 146 (2009) 466–476.
[4] X.Z. Chen, Z.H. Luo, W.C. Yan, Y.H. Lu, I.S. Ng, Three-dimensional CFD-PBM coupled model of the temperature fields in fluidized bed polymerization reactors, AIChE J. 57 (2011) 3351–3366.
[5] W.C. Yan, Z.H. Luo, Y.H. Lu, X.D. Chen, A CFD-PBM-PMLM integrated model for the gas–solid flow fields in fluidized bed polymerization reactors, AIChE J. 58 (2012) 1717–1732.
[6] R. Fan, D.L. Marchisio, R.O. Fox, Application of the direct method of moments to polydisperse gas–solid fluidized beds, Powder Technol. 139 (2004) 7–20.
[7] R. Fan, R.O. Fox, M.E. Muhle, Role of intrinsic kinetics and catalyst particle size distribution in CFD simulation of polymerization reactors, in: ECI Conference on The 12th International Conference on Fluidization-New Horizons in Fluidization Engineering: Vancouver (Canada), 2007. pp. 993–1000.
[8] P. Pei, K. Zhang, D.S. Wen, Comparative analysis of CFD models for jetting, fluidized beds: the effect of inter-phase drag force, Powder Technol. 221 (2012) 114–122.
[9] P. Li, X.Y. Lan, C.M. Xu, G. Wang, C.X. Lu, J.S. Gao, Drag models for simulating gas–solid flow in the turbulent fluidization of FCC particles, Particuology 7 (2009) 269–277.
[10] C. Loha, H. Chattopadhyay, P.K. Chatterjee, Assessment of drag models in simulating bubbling fluidized bed hydrodynamics, Chem. Eng. Sci. 75 (2012) 400–407.
[11] C.Y. Wen, Y.H. Yu, Mechanics of fluidization, Chem. Eng. Prog. Sympos. Series 62 (1966) 100–111.
[12] M. Syamlal, T.J. O'Brien, Computer simulation of bubbles in a fluidized bed, AIChE Sympos. Series 85 (1989) 22–31.
[13] D. Gidaspow, Multiphase Flow and Fluidization: Continuum and Kinetic Theory Descriptions, Academic Press, Boston, 1994.
[14] T. McKeen, T. Pugsley, Simulation and experimental validation of a freely bubbling bed of FCC catalyst, Powder Technol. 129 (2003) 139–152.
[15] N. Yang, W. Wang, W. Ge, J. Li, CFD simulation of concurrent-up gas-solid flow in circulating fluidized bed with structure-dependent drag coefficient, Chem. Eng. J. 96 (2003) 71–80.
[16] N. Yang, W. Wang, W. Ge, J. Li, Simulating of heterogeneous structure in a circulating fluidized bed riser by combining the two-fluid model with the EMMS approach, Ind. Eng. Chem. Res. 43 (2004) 5548–5561.
[17] W. Wang, J. Li, Simulation of gas-solid two-phase flow by a multi-scale CFD approach: extension of the EMMS model to the sub-grid scale level, Chem. Eng. Sci. 62 (2007) 208–231.
[18] J. Wang, W. Ge, J. Li, Eulerian simulation of heterogeneous gas–solid flows in CFB risers: EMMS-based sub-grid scale model with a revised cluster description, Chem. Eng. Sci. 63 (2008) 1553–1571.
[19] J. Wang, Y. Liu, EMMS-based Eulerian simulation on the hydrodynamics of a bubbling fluidized bed with FCC particles, Powder Technol. 197 (2010) 241–246.
[20] J. Wang, Q. Zhou, K. Hong, W. Wang, J. Li, An EMMS-based multi-fluid model (EFM) for heterogeneous gas-solid riser flows: Part II. An alternative formulation from dominant mechanisms, Chem. Eng. Sci. 75 (2012) 349–358.
[21] K. Zhang, J.Y. Zhang, B.J. Zhang, J. Yates, CFD model of dense gas–solid systems in jetting fluidized beds, Chem. Res. Chinese Univ. 18 (2002) 117–120.
[22] K. Zhang, P. Pei, S. Brandani, H. Chen, Y. Yang, CFD simulation of flow pattern and jet penetration depth in gas-fluidized beds with single and double jets, Chem. Eng. Sci. 68 (2012) 108–119.
[23] A. Nikolopoulos, N. Nikolopoulos, A. Charitos, P. Grammelis, E. Kakaras, High-resolution 3-D full-loop simulation of a CFB carbonator cold model, Chem. Eng. Sci. 90 (2013) 137–150.
[24] W.C. Yan, J. Li, Z.H. Luo, A CFD-PBM coupled model with polymerization kinetics for multizone circulating polymerization reactors, Powder Technol. 213 (2012) 77–87.
[25] X.Z. Chen, D.P. Shi, X. Gao, Z.H. Luo, A fundamental CFD study of the gas–solid flow field in fluidized bed polymerization reactors, Powder Technol. 205 (2011) 276–288.
[26] S. Ergun, Fluid flow through packed columns, Chem. Eng. Prog. 48 (1952) 89–94.
[27] L.G. Gibilaro, R. Di Felice, S.P. Waldram, P.U. Foscolo, Generalized friction factor and drag coefficient correlations for fluid–particle interactions, Chem. Eng. Sci. 40 (1985) 1817–1823.
[28] W. Du, X.J. Bao, J. Xu, W.S. Wei, Computational fluid dynamics (CFD) modeling of spouted bed: assessment of drag coefficient correlations, Chem. Eng. Sci. 61 (2006) 1401–1420.
[29] S. Patankar, Numerical Heat Transfer and Fluid Flow, Hemisphere Publishing Corporation, 1980.
[30] C.K.K. Lun, S.B. Savage, D.J. Jeffrey, N. Chepurniy, Kinetic theories for granular flow-inelastic particles in couette-flow and slightly inelastic particles in a general flow field, J. Fluid Mech. 140 (1984) 223–232.
[31] C.J. Chai, G.L. Zhang, Chemical Engineering Fluid Flows and Heat Transport, Chemical Engineering Press (Chinese), Beijing, 2004.
[32] P. Lettieri, R.D. Felice, R. Pacciani, O. Owoyemi, CFD modeling of liquid fluidized beds in slugging mode, Powder Technol. 167 (2006) 94.
[33] D.P. Shi, Z.H. Luo, A.Y. Gao, Numerical simulation of the gas–solid flow in fluidized-bed polymerization reactors, Ind. Eng. Chem. Res. 49 (2010) 4070–4079.
[34] Y. Jin, J.X. Zhu, Z.W. Wang, Z.Q. Yu, Fluidization Engineering Principles, Tsinghua University Press, Beijing, 2001.
[35] J. Li, H. Weinstein, An experimental comparison of gas backmixing in fluidized beds across the regime spectrum, Chem. Eng. Sci. 44 (1989) 1697–1705.
[36] H. Hatzantonis, A. Goulas, C. Kiparissides, A comprehensive model for the prediction of particle-size distribution in catalyzed olefin polymerization fluidized-bed reactors, Chem. Eng. Sci. 53 (1998) 3251–3267.
[37] W. Ranz, W.R. Marshall, Evaporation from drops, Chem. Eng. Prog. 48 (1952) 141–146.
[38] J.J. Zacca, W.H. Ray, Modeling of the liquid phase polymerization of olefins in loop reactors, Chem. Eng. Sci. 48 (1993) 3743–3765.

Please cite this article in press as: Y. Yao et al., 3D CFD-PBM modeling of the gas–solid flow field in a polydisperse polymerization FBR: The effect of drag model, Advanced Powder Technology (2014), http://dx.doi.org/10.1016/j.apt.2014.04.001